Formation of Y-Ti-O nanoclusters in nanostructured ferritic alloys: A first-principles study

Yong Jiang,[1,2] John R. Smith,[1] and G. R. Odette[1,2]
[1]*Department of Materials, University of California-Santa Barbara, Santa Barbara 93106, USA*
[2]*Department of Mechanical Engineering, University of California-Santa Barbara, Santa Barbara 93106, USA*
(Received 17 October 2008; published 6 February 2009)

Density-functional theory (DFT) calculations have been performed to study the atomic scale energies, structures, and formation mechanisms of dissolved Y, Ti, and O solutes and small Y-Ti-O nanoclusters (NCs) in a bcc Fe lattice. Key results include the following observations. The Y and O are dissolved during mechanical alloying of Y_2O_3 with metal powders by ball milling, which provides the large requisite solution energy of about 4 eV per yttria atom. The solution energies of substitutional Y as well as interstitial O, which are referenced to elemental Y and solid FeO, respectively, are also high. Bound O-O, Y-O, and Ti-O pairs decrease the system energy relative to the isolated solutes and constitute the basic building blocks for NCs. The lowest energy configuration for a Y_2TiO_3 NC is 5.11 eV less than the total energy of the dissolved solutes. Our DFT calculations show that Y-Ti-O NC formation can take place without the energetic assistance of pre-existing vacancies. This conclusion is significant since excess vacancies are not a persistent thermodynamic-energetic constituent of the Fe-Y-Ti-O system and will quickly annihilate at dislocations during high-temperature powder consolidation.

DOI: 10.1103/PhysRevB.79.064103 PACS number(s): 81.20.Ev, 81.30.Mh, 61.72.J−

I. INTRODUCTION AND BACKGROUND

The challenges of meeting the rapidly growing demand for cleaner energy will require developing new high temperature, high performance structural alloys with outstanding properties that are sustained under long-term service in severe environments. As described in a recent review paper,[1] this is especially true for advanced fission and fusion energy systems that must manage high levels of radiation damage, including both hundreds of displaced atoms and, for fusion applications, high concentrations of transmutation product helium. In this paper we address some fundamental issues facing a revolutionary class of nanodispersion strengthened ferritic alloys (NFAs) that show enormous promise of meeting these challenges. As discussed in Ref. 1, NFAs contain an ultrahigh density of Y-Ti-O enriched nanofeatures that, along with fine grains and high dislocation densities, provide remarkably high creep strength far exceeding that for other ferritic alloys.[1] The nanofeatures also enhance the self-healing of radiation displacement damage and trap helium in harmless, nanometer-scale interface bubbles, thereby suppressing void swelling, severe degradation of fracture toughness, and loss of creep rupture strength.[1,2] The nanofeatures are remarkably stable, both at high temperatures and after large neutron irradiation doses.[1]

NFAs contain Fe-12 to 14% Cr, 1%–3% W along with small quantities of Y, O, and Ti that are the primary precipitation strengthening solutes.[1] NFAs are processed by mechanically alloying (MA) metallic (Fe, Ti, Cr, W) and Y_2O_3 oxide powders by ball milling. MA dissolves the Y_2O_3 constituents, which then precipitate along with Ti during high-temperature processing, at typical temperatures of about 1150 °C.[1,3] The mechanisms of solute dissolution during MA are not well understood, but we believe that repeated fracture and, ultimately, slicing of the fragmented oxides by dislocations during the severe deformation produced by ball milling plays an important role.[4] Both the dissolved O and Y in the MA powders are far in excess of concentrations that are introduced by typical near-equilibrium solidification processes.

The nanofeatures have been studied by small-angle neutron scattering (SANS),[1,3,5] three-dimensional atom probe tomography (APT) (Refs. 1 and 6–9) and transmission electron microscopy (TEM).[1,10–12] The nanofeatures form very rapidly, at number densities, sizes, and characteristics (compositions and structures) primarily dictated by the processing temperature history and alloy composition.[1,3] However, the precise natures of various nanofeatures are not yet well understood. They appear to range from coherent solute enriched clusters, or GP-type zones, with complex shell structures, as found by APT,[10] to near stoichiometric complex oxides, such as Y_2TiO_5 and $Y_2Ti_2O_7$, as found in some SANS (Refs. 1 and 3) and TEM studies.[1,10–12]

In this work we use *ab initio* electronic structure methods to characterize the solution energetics of Y, Ti, and O in Fe and the earliest stages of solute clustering. The sizes and complexity of the actual nanofeatures themselves are far beyond the direct capabilities of such calculations. However, the basic energetic properties of the solutes dissolved in Fe, and very small solute nanoclusters (NCs), are needed to understand the larger nanofeature structures and compositions as well as the thermokinetics of their formation and long-term stability at elevated temperatures. In this regard, our work extends and complements a recent study by Fu *et al.*,[13] which emphasized the role of vacancies in the high excess O contents in NFA, Y-Ti-O clustering and cluster stability.

To begin it is important to establish a proper physical framework for conducting and interpreting the *ab initio* DFT calculations. Yttrium is a very large atom and is basically insoluble in the Fe lattice. However, very high, nonequilibrium supersaturations (concentrations above the solubility limit) of Y are introduced by MA. Interstitial O in equilibrium with FeO also has a very low solubility in Fe. However, high supersaturations of O are also mechanically mixed into the as-milled powders at concentrations of up to 0.3 at. %,

or more. Note very high supersaturations of N and C can also be dissolved in Fe by MA.[4,14]

Ball milling also generates very high dislocation densities[1,3,15] and produces excess vacancies.[16] Here we formally define vacancies as point defects composed of relaxed atom positions around a distinct unoccupied lattice sites. Both excess vacancies and dislocations accelerate solute diffusion rates as well as nanofeature nucleation and growth rates. While the excess vacancy concentrations in the milled powders are not known, it is likely that they remain far lower than the concentrations of the dissolved Y, Ti and O, that total order 1%, for reasons discussed below. Vacancies are also annihilated during MA by (gliding) dislocations and possibly by self-interstitial atoms, hence, are expected to approach steady-state concentrations. Moreover, excess vacancies present after MA are not a persistent thermodynamic-energetic constituent of the Fe-Y-Ti-O system following hot consolidation, when dissolved O remains supersaturated to very high concentrations,[6–8] after most of the excess vacancies have been annihilated or precipitated into larger vacancy clusters or gas bubbles.[17] For example, assuming a dislocation sink density of $10^{15}/m^2$, and using the high O-V complex migration energy suggested by Fu *et al.*[13] of 1.55 eV, the vacancy relaxation time is $<10^{-5}$ s at 1150 °C.[18] Further perspective on high-temperature vacancy annihilation is provided by considering the fact that of order 26%, or more, of porosity is eliminated during powder consolidation.[19]

The issue of the vacancies is to some extent semantic. For example, we show that the O-O pair that shares a lattice site represents a low solute energy configuration. Some may "see" the lattice site as a vacancy. However, it is no more appropriate to consider the vacancy energy in this case than it would be to consider a vacancy in evaluating the energy of a self interstitial atom defect, or a substitutional solute for that matter. Note, as discussed further below, these comments are not meant to dismiss the important role of vacancies in NC and nanofeature formation kinetics.

The question remains about why high concentrations of O persist in solution even after hot consolidation. The equilibrium concentration of O in unalloyed Fe is controlled by FeO and is in the range of atom parts per million (appm) even at high temperatures. The possible fates of the O in the alloy powders during hot consolidation are governed by a combination of thermodynamic and kinetic factors that include: (1) forming the nanofeature transition phase solute clusters and complex Y-Ti oxides; (2) forming coarser scale equilibrium incoherent alloy oxides of Y, Ti, Cr, and W, in decreasing order of stability; (3) remaining in supersaturated solution. While coarser scale TiO_2 is observed in NFAs,[1,12] it appears that kinetic factors, such as large activation barriers for nucleation of incoherent precipitates limit the formation rates of the larger equilibrium oxide phases relative to the non-equilibrium nanoscale transition phase and complex oxide nanofeatures.[20] We will also show below that the solution energy for O-O pairs is lower than that of two octahedral interstitial O atoms, and in conjunction with O-O-Ti complexes, this may partly rationalize the persistence of high concentrations of dissolved O. Note the formation of nanofeatures also partially depletes the dissolved O and Ti further reducing the thermodynamic driving force for TiO_2 formation.

Based on this framework we address the following specific questions:

(i) What are the energy differences between Y and O solutes dissolved in Fe relative to Y_2O_3 (that is, what is the minimum-energy expenditure in MA needed to dissolve the solutes)?

(ii) What are the energy differences between the solutes Y, Ti and O dissolved in Fe relative to their reference states (that is, what are their solution energies)?

(iii) What are the energies of small, coherent NCs of Y, Ti and O relative to the solution energies (that is, what is the driving force for solute clustering)?

(iv) What is the nature of the bonding and bond energies of small solute NCs that can provide insight on how such "building blocks" can be assembled into larger nanofeatures?

II. COMPUTATIONAL METHOD

We employ density-functional theory (DFT) calculations to investigate the energetics and electronic structures of dissolved Y, Ti, and O solutes and NC formation. These calculations show that dissolution of Y_2O_3 into the Fe matrix requires a large amount of energy, primarily due to the high stability of Y_2O_3; ball milling provides this energy. Once dissolved, the solutes experience large energy difference driving forces to form NCs. There are a large number of NC configurations with lower energy than the dissolved solutes. Thus considerable effort is directed at finding the lowest NC energy compositions and configurations. We also show that additional insight can be gained by examining electron-density redistributions associated with the dissolved solutes and solute pairs.

We employ the DFT simulation package VASP (Ref. 21) for all energy calculations. These calculations are performed with pseudopotentials generated with the projector-augmented wave (PAW) method.[22] The semicore $3p$ orbitals of Ti and $4s$ and $4p$ orbitals of Y are all treated as valence electrons. The generalized gradient approximation [PBE (Ref. 23)] is used to describe exchange-correlation effects. For electron eigenvalues and Brillouin-zone integrations, a plane-wave cutoff energy of 400 eV and a uniform $2\times2\times2$ Monkhorst-Pack k mesh are used for the $4\times4\times4$ supercell of bcc Fe containing 128 atoms. Structural relaxations were carried out until all force components converged to zero within 0.01 eV/Å. Several fully spin-polarized ground-state properties of pure Fe (bcc), Y, and Ti (hcp), and O (FeO) (xtal structure) are calculated and as summarized in Table I, show good agreement with available experimental data.[24–29]

We define the solution energies for Y, Ti, and O at different sites in the Fe host as

$$E^s_{\mathrm{Y/Ti/O}} = E_{\mathrm{Fe+Y/Ti/O}} - n_{\mathrm{Fe}}\mu_{\mathrm{Fe}} - \mu_{\mathrm{Y/Ti/O}}. \quad (1)$$

Here, $E_{\mathrm{Fe+Y/Ti/O}}$ is the total energy of the $4\times4\times4$ supercell of bcc Fe embedded with a single isolated solute atom (Y, Ti, or O) at either a substitutional or an interstitial site, n_{Fe} is the total number of Fe atoms in the supercell.

The use of the chemical-potential notation, μ_i, provides consistency with convention in the large DFT literature.

TABLE I. Some fully spin-polarized ground-state properties of hcp Ti and Y, bcc Fe, and FeO.

	Ti	Expt.[a,b]	Y	Expt.[c]	Fe	Expt.[d,e]	FeO	Expt.[f]
B (GPa)	111.1	110	40.4	41	168.8	173	178	152.3
a (Å)	2.945	2.951	3.659	3.647	2.835	2.867	4.31	4.33
c (Å)	4.646	4.686	5.677	5.731				
a/c	1.578	1.588	1.552	1.571				

[a]Reference 24.
[b]Reference 25.
[c]Reference 26.
[d]Reference 27.
[e]Reference 28.
[f]Reference 29.

However, our 0 K energy calculations only account for atomic bonding energies and do not include either the effects of entropy ($S=0$ at 0 K), or the temperature dependence of enthalpy and entropy contributions to the free energies of solution. While this precludes a quantitative thermodynamic assessment pertinent to high temperatures, we believe that our qualitative conclusions are robust.

III. RESULTS

Table II summarizes the calculated solution energies for both substitutional and various interstitial solute configurations. We follow the schematic description given by Olsson *et al.* in Fig. 4 of Ref. 30 for all interstitials: the $\langle 110\rangle_{\text{Fe-S}}$ configuration has a Fe-solute pair aligned along $\langle 110\rangle$; and the $\langle 110\rangle_{\text{Fe-Fe}} \perp S_{\text{sub}}$ configuration has a Fe-Fe pair aligning along $\langle 110\rangle$ with the solute atom at a corner substitutional site. Other interstitial configurations were found to converge to these two structures upon full lattice relaxation. The Fe self-interstitial and vacancy energies are also computed and compared to previously published results.[13,30,31]

As expected, substitutional Ti and Y have the lowest energy, while the lowest energy site for O is an octahedral interstitial (O_{int}) position. The O_{int} solution energy of 1.41 eV compares favorably with the value of 1.45 eV found by Fu *et al.*[13] Yttrium is essentially insoluble in Fe even without the formation of the $Fe_{17}Y_2$ phase. For example, ignoring effects of finite temperature on enthalpy and excess entropy and changes in the Y crystal structure upon dissolution, the solution energy of 2.02 eV limits the solubility of Y in Fe at 1150 °C in equilibrium with elemental Y to about 7×10^{-8}. The negative solution energy of Ti implies that equilibrium solubility levels in Fe are limited by the intermetallic Fe_2Ti phase.

TABLE II. Point defect formation and solution energies (eV) in bcc Fe. For interstitial sites, we follow the schematic description given by Olsson *et al.* (Ref. 30). Numbers shown in italics correspond to the most energy-favored sites when available. Negative values correspond to exothermic formation energies.

	Fe	Ti	Y	O
Substitutional		−0.80	2.02	2.99
Octahedral	5.27 (5.29,[a] 4.94[b])	5.30	8.99	1.41
Tetrahedral	4.45 (4.15[b])	4.76	8.38	3.26
$\langle 110\rangle_{\text{Fe-S}}$	4.04 (4.02,[a] 3.64[b])	4.51	8.30	2.66
$\langle 110\rangle_{\text{Fe-Fe}} \perp S_{\text{sub}}$		3.07	5.64	7.18
$\langle 110\rangle_{\text{Fe-Fe}}$-$S_{\text{sub}}$		3.80	6.24	4.26
Vacancy	2.13(2.15,[a] 2.07,[b]1.95[c])			

[a]Reference 30.
[b]Reference 31.
[c]Reference 13.

The substitutional O (O_{sub}) has the highest solution energy of 2.99 eV, compared to 1.41 eV for the octahedral interstitial O (O_{int}). However, the system energy decreases 1.0 eV when the O_{sub} atom relaxes from the lattice site by 1.12 Å in the [001] direction. For convenience we will refer to this configuration as a relaxed O_{int} vacancy (O_{int}-V) pair, with a binding energy of ≈1.55 eV relative to separated O_{int} and V. This binding energy compares favorably with the corresponding value of ≈1.45 eV reported by Fu *et al.*[13] However, the O_{int}-V pair is energetically favorable compared to O_{int} only if a pre-existing vacancy energy of ≈2.13 eV is included in the balance. As noted previously, however, excess vacancies are not a persistent thermodynamic-energetic constituent of the Fe-Y-Ti-O system. In decreasing order the system energies are: separated V+O_{int}, 3.54 eV; O_{sub}, 2.99; O_{int}-V pair, 1.99 eV; O_{int}, 1.41 eV. Again, solutes can only reconfigure, while *excess* vacancies and their corresponding energies can be entirely eliminated by annihilation, in this case reducing the system energy by 0.58 eV per annihilated vacancy (from O_{int}-V pair to O_{int}). Thus our further solute cluster energy calculations described below examine formation energies of NCs without the presence of vacancies.

An analysis of differential electron charge densities is useful to gain a better qualitative understanding of the bonding character. Figure 1 shows the spatial redistributions of electron density of an octahedral interstitial O, compared to that for a substitutional Y and Ti. The electron-density redistribution is evaluated as the difference between the electron density of the solute-containing Fe solid solution ($4\times4\times4$ bcc supercell) and the superposition densities of the Fe host and the free solute atom. As seen in Fig. 1(a), strong electronic bonding of O to Fe is evident. The O *sp* orbitals getter electrons, primarily from the first- and second-nearest neighboring Fe dz^2-like orbitals. Both the charge accumulation and

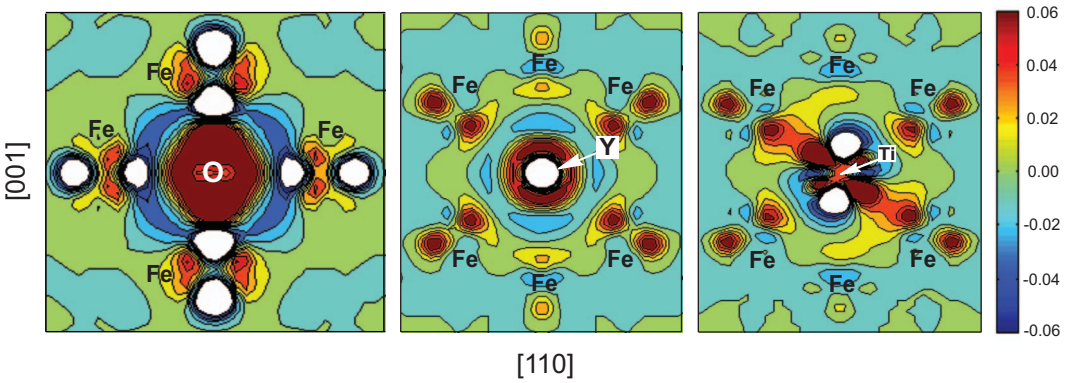

FIG. 1. (Color) Differential electron densities in the units of electrons/Å^3 in the (110) plane for an octahedral interstitial O, a substitutional Y, and substitutional Ti, all in bcc Fe (from left to right). The white regions have density values of less than −0.06 e/Å^3.

depletion regions are spatially confined around O. The important role of magnetism of the host Fe lattice in confining the local O charge, as discussed in Ref. 13, can be revealed by comparing spin-polarized and unpolarized total electron densities. Consistent with the conclusion of Fu *et al.*, the Fe-O bond has a significant ionic character. Because of the shorter distance of O to the two-body-centered Fe atoms than from the four corner Fe atoms, the charge distribution at the octahedral O site is not spherical in the [010]–[100] plane, but rather is extended along the [001] direction. While the Fe-O_{int} [011] bond lengths are basically unchanged by relaxation, the [001] bond lengths increase by about 27%.

In contrast, the substitutional Y and its surrounding Fe atoms lose some charge in their interstitial regions [Fig. 1(b)], suggesting that the bonding is fairly weak, having a mixed ionic-metallic character. The strain energy accompanying a lattice expansion of ~5.9%, which is expected from the significantly larger atomic radius for Y compared to Fe [≈23% larger for elemental Y versus Fe (Ref. 32] also contributes to the large 2.02 eV solution energy for substitutional Y. In the case of substitutional Ti in Fe [Fig. 1(c)], *d*-band splitting occurs at the Ti site: Ti e_g-like orbitals (dz^2,dx^2+y^2) give electronic charge to not only Fe dz^2-like orbitals and also to Ti t_{2g}-like orbitals (*dxz*, *dyx*, or *dyz*). The later two orbitals even hybridize, giving a partially covalent character. The stronger Fe-Ti electronic bonding results in a negative (exothermic) energy of solution of −0.80 eV, in spite of a small lattice strain (expansion) of ≈1.5%.

We choose the bulk oxide Y_2O_3 and the bulk metal Ti as the O, Y, and elemental Ti sources to evaluate the energy change in dissolving Y_2O_3 and Ti into Fe as

$$\Delta E_{\mathrm{MA}} = (2E_{\mathrm{Fe+Y}} + E_{\mathrm{Fe+Ti}} + 3E_{\mathrm{Fe+O}}) - n_{\mathrm{Fe}}\mu_{\mathrm{Fe}} - \mu_{\mathrm{Y_2O_3}} - \mu_{\mathrm{Ti}}. \tag{2}$$

Here $E_{\mathrm{Fe+O}}$, $E_{\mathrm{Fe+Y}}$, or $E_{\mathrm{Fe+Ti}}$ is the total energy of the $4\times4\times4$ bcc supercell of Fe containing a single octahedral interstitial O, or a substitutional Y or Ti atom. The $\mu_{\mathrm{Y_2O_3}}$ for Y_2O_3 is computed using the calculated equilibrium lattice constant of 10.71 Å [compared to the experimental value of 10.604 Å (Ref. 33)]. The total-energy cost of dissolving Y_2O_3 and Ti into Fe is determined to be ΔE_{MA}=19.98 eV. The very large energy required per Y_2O_3+Ti addition suggests that a high-energy process, such as MA, is needed to achieve the dissolution of Y, Ti, and O in Fe.

The energy differences between solutes dissolved in Fe versus in Y-Ti-O clusters are the driving force for NC formation. The energy (ΔE_C) change in forming small clusters ($Y_xTi_yO_z$) is obtained as

$$\Delta E_C(\mathrm{Y}_x\mathrm{Ti}_y\mathrm{O}_z) = E_{\mathrm{Fe+(Y}_x\mathrm{Ti}_y\mathrm{O}_z)} - [(xE_{\mathrm{Fe+Y}} + yE_{\mathrm{Fe+Ti}} + zE_{\mathrm{Fe+O}}) - \Delta n_{\mathrm{Fe}}\mu_{\mathrm{Fe}}]. \tag{3}$$

The Δn_{Fe} accounts for the difference in the number of Fe atoms between the two solute configurations: $E_{\mathrm{Fe+Y}_x\mathrm{Ti}_y\mathrm{O}_z}$ and ($xE_{\mathrm{Fe+Y}}+yE_{\mathrm{Fe+Ti}}+zE_{\mathrm{Fe+O}}$). Based on ΔE_C as a criterion, one can search for the energetically optimized composition and configuration of the NCs and establish the minimum-energy initial cluster growth sequence. Using insights from Table II, we consider only substitutional Y and Ti, and both substitutional and interstitial O, in evaluating the energetics of the cluster formation. Note pair configurations at the second-nearest-neighbor (2NN) position are also treated since the distances to first (1NN) and 2NN differ by only about 15% in the bcc lattice.

A NC can form only if the corresponding ΔE_C is negative. Table III summarizes the calculated ΔE_C for 18 candidate pair-cluster configurations in bcc Fe. Only O_{int}+O_{sub} and metal solute-O pairs are bound and with the exception of the Y_{sub} and O_{sub} pair, all other substitutional solute-solute pair interactions are repulsive. Thus we conclude that the solutes O-O, Ti-O, and Y-O pairs with attractive interactions act as the basic building blocks for the initial formation of NCs. The lowest energy pair is found to be the O-O with an initial configuration (before relaxation) of O_{int}-O_{sub}. After relaxation, the two O atoms align along the ⟨010⟩ direction spanning the cube center. This relaxation produces a large negative (binding) energy change for the O-O pair of ΔE_C(O-O)=−1.29 eV, relative to a reference state of two isolated O_{int} atoms. It is best to view the net relaxed O-O configuration as a split solute interstitial pair with two O atoms sharing a single lattice site, analogous to a split-dumbbell self-interstitial atom defect.[31] The O_{int}-O_{int} interaction is repulsive, with an energy of 0.4 eV.

The O_{sub} and O-V configurations may result from the O reactions with vacancies created during MA; alternatively,

TABLE III. Calculated ΔE_C for various pair configurations in bcc Fe. We consider substitutional Y and Ti, and O_{sub} and O_{int} only, to form pair clusters in both first- and second-nearest neighbors in the bcc lattice, 1NN and 2NN. Here the definition of 1NN and 2NN is broadened to include nearest and next-nearest neighbors of O_{int}. A negative ΔE_c indicates a total-energy reduction resulting from an energy-favored cluster formation.

	ΔE_C (eV)	
Initial pair configurations	1NN	2NN
$Y_{sub}+Y_{sub}$	0.20	0
$Y_{sub}+Ti_{sub}$	0.28	0.15
$Ti_{sub}+Ti_{sub}$	0.29	0.15
$Y_{sub}+O_{sub}$	−0.33	−0.30
$Ti_{sub}+O_{sub}$	0.82	1.69
$O_{int}+Ti_{sub}$	−0.27	−0.55
$O_{int}+Y_{sub}$	0.28	−0.85
$O_{int}+O_{sub}$	−1.29	0.19
$O_{sub}+O_{sub}$	2.03	
$O_{int}+O_{int}$	0.40	

O_{sub} or O-V and O-O pairs, as well as substitutional Ti and Y, could be easily produced during MA itself since during mixing the volume per atom in Y_2O_3 replaces approximately the same the atomic volume of Fe, and since the energy cost of O_{sub} versus O_{int} is small compared to the total energy of MA. However, any O_{sub}, or lower energy O-V pair, would quickly transform to an O-O pair, with a lower solution energy. Further, $O_{int}+O_{int}+$*thermal* vacancy reactions would continue to produce additional O-O pairs at high consolidation temperatures. Thus the initial state in the milled powders is expected to be substitutional Ti and Y and an unknown mixture of O_{int} and lower energy O-O pairs. Note that in contrast to Ref. 13 we found three attractive Y-O bond configurations.

Figure 2 shows the calculated differential electron densities of an O-O pair, a Ti-O, and a Y-O pair in bcc Fe. All contours are plotted to the same scale as Fig. 1. Figure 2(a) shows that the O atoms in the O-O pair are both negatively charged and are separated by a region of electron charge depletion at the shared lattice site that can be considered a relaxed O_{sub} plus O_{int}. Of course the lattice site, and the absence of a Fe atom, must be present to be shared; however, the lattice site no more represents a vacancy defect than if it were occupied by a substitutional solute. The O atoms in the O-O pair are more polarized compared to the clearly ionic O_{int} configuration, where the latter's [001] Fe-O bonds are slightly elongated while the four [110] bonds are shortened by about the same amount (~2%) increasing the bond strength. As seen in Fig. 2(b) or 2(c), the density difference plots for substitutional Ti or Y in a Ti-O or Y-O pair show some similarities to those for the corresponding isolated solute atoms (Fig. 1). The oppositely charged Ti and O are suggestive of an attractive ionic pair interaction reducing the total energy by 0.55 eV at the 2NN distance. In contrast, the both atoms in the Y-O nearest-neighbor pair acquire a net negative charge. Thus the binding energy in this configuration is most likely due to reductions in lattice strains

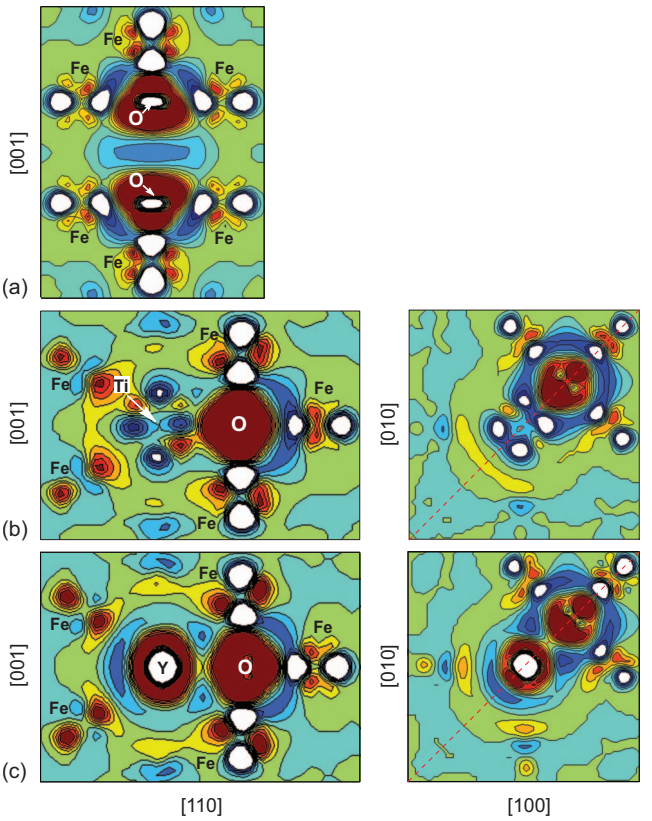

FIG. 2. (Color) Differential electron densities in the same scale for (a) an O-O, (b) a Ti-O, and (c) a Y-O pair, in bcc Fe. Note the Ti-O and Y-O pairs are both in the 2nd-NN distance. The red dash lines in (b) and (c) correspond to the positions of the contour planes on the left. The white regions have density values of less than −0.06 e/Å^3.

Next we construct larger clusters by adding solutes to the bound O-O pair, the lowest energy pair configuration in Table III. Figure 3 shows the sites for the third atom to form a triatom solute-O-O cluster. Candidate locations for the third atom include three substitutional sites for Y, Ti, and O and three interstitial sites for O. Thus a total of 12 tricluster configurations are treated to search for the lowest energy configuration. The energy-minimized tricluster is O-O-Y (the O-O-Y notation indicates the sequence of solute additions; of

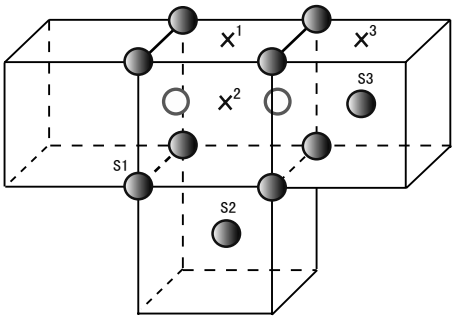

FIG. 3. Sites considered for the formation of a Tri-cluster from a O-O pair cluster, including three substitutional sites (S1-S3) for Y, Ti, or O and three interstitial sites (X^1-X^3) for O.

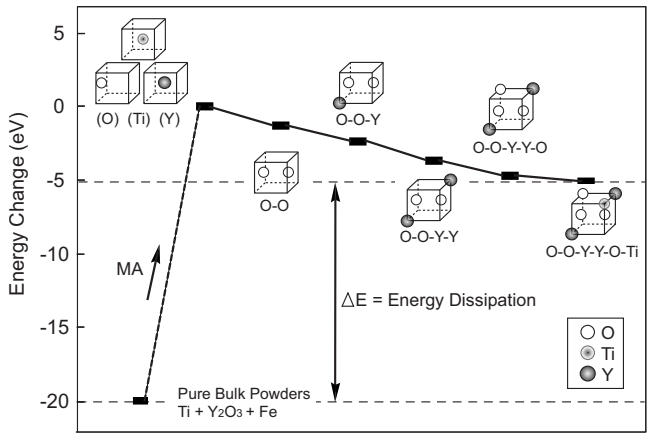

FIG. 4. Energy changes associated with mechanical alloying processing and subsequent precipitations of (Y-Ti-O) nanoclusters in bcc Fe.

course, the energy of a cluster is independent of the construction sequence), with the Y at the S1 site. Note, this result may be consistent with the observation that Y-O is enriched in the core of the nanofeatures that is surrounded by a Ti-O shell.[9] The corresponding ΔE_C(O-O-Y)=−2.36 eV, is −0.50 eV lower than the second lowest energy configuration (O-O-O_{S3}) and −0.52 eV lower than the third lowest energy configuration (O-O-Ti_{S1}). However, both of these other NC configurations are energetically accessible. Following the same procedure, further calculations are carried out to larger sizes up to one Ti atom beyond the smallest stoichiometric Y_2O_3 unit NC. The energy-minimized configurations and associated energy changes are plotted in Fig. 4. The total-energy change for the largest NC is ΔE_C(O-O-Y-Y-O-Ti) =−5.11 eV. This ΔE_C represents a very large energy driving force for Y-Ti-O NC formation, even absent excess vacancies.

IV. DISCUSSION AND SUMMARY

We present here a quantitative model for Y, Ti and O solution energies and the corresponding energy reductions associated with the initial formation of Y-Ti-O NCs. Where they can be compared, our DFT results are consistent with those of Fu *et al.*[13] In contrast to that work, however, we argue that excess vacancies should not be considered to be a persistent thermodynamic-energetic component of the Fe-Y-Ti-O system. Within the assumptions of our calculations based on changes in the system bonding energy, we show unambiguously that formation of NCs from supersaturated solid solutions decreases the system energy.

The observation of the energy advantage of the bound O-O pair warrants further discussion. Such clusters would significantly enhance O solubility relative to the O_{int} levels. In principal the O-O pairs would be the equilibrium dissolved O species. However, formation of the O-O pairs may be kinetically constrained under normal circumstances because of low concentrations of bulk O in equilibrium with surface oxide scales, and the requirement for a thermal vacancy to convert two O_{int} to this configuration in the absence of MA. In contrast, mixing high concentrations of O into solution by MA favors strongly the formation of the O-O pairs, thereby lowering the thermodynamic driving force of internal nucleation and growth of incoherent equilibrium oxides. Lower O-O energies may provide a partial rationalization for the very high concentrations of dissolved O that are observed in NFAs. Interaction of dissolved O-O with Y and Ti would further enhance this effect. Notably, such Ti-O and Y-O associations are often observed in APT studies.[6–9] However, an important caveat is that the effects of finite temperature have not been considered in the preceding analysis.

Fu *et al.*[13] suggest that O trapping in O-V pairs is also a rate controlling mechanism for nanofeature formation and aging kinetics. Note, O diffusion in NFAs is also affected by the dissolved solutes (Cr, W, and Ti). However, O and vacancies are highly mobile at high consolidation temperatures, even for the O-V complex migration energy of 1.55 eV reported by Fu *et al.*[13] Thus the excess vacancies annihilate at high temperatures, and it is much more likely that the continued evolution of the nanofeatures is controlled by Ti and Y diffusion as well as NC interface properties, Y solubility, and excess O concentrations, rather than the O diffusion rate. Further, Table III also shows that there are a number of energetically accessible solute O configurations that could provide lower energy migration paths. Indeed, the O-O split interstitial pairs may be especially mobile, emulating split self-interstitial atoms with similar configurations.[31]

Our examples of the energetics of NC formation neither constitute a rigorous thermodynamic analysis for the Fe-Y-Ti-O system, nor a precise model for nanofeature formation, since the latter involve many additional complexities. These models can and will be extended to develop a thermodynamic framework for the Fe-Y-Ti-O system (see example for the Al-Ni system in Ref. 34). However, we believe that our DFT clustering energy results provide strong qualitative evidence that a wide range of coherent NC with nonstoichiometric compositions can form based on the aggregation of the basic Y-Ti-O building blocks, including clusters that are richer in Ti.

As is usually the case in the formation of nonequilibrium transition phases, the decomposition path selection is controlled by kinetic as well as thermodynamic factors (see Ref. 20). For coherent NCs and nanofeatures, important thermodynamic factors include the coherency strains and interface energies, as well as the net chemical free-energy differences driving precipitation.[35] The solution energies for Ti are much lower than for Y (Table III) consistent with the differential electron-density maps shown in Fig. 1 suggesting stronger Ti-Fe versus Y-Ti bonds. These results indicate that Ti, or perhaps Ti-terminated oxides, would provide more favorably bonded interfaces with the Fe matrix compared to Y and Y oxides, possibly rationalizing the observation of Y-Ti-O enriched nanofeature cores surrounded by Ti-O rich shells.[9] Finally, we believe that a combination of low-energy nanofeature coherent interface energies, very low solubility of Y and persistent excess O concentrations partly explain the remarkable thermal stability of the nanofeatures. We will explore these hypotheses in future studies.

In closing, we return briefly to the potential role of vacancies in NC and nanofeature formation. While we believe that

so-called excess vacancies need (and should) not be considered to be a persistent alloy constituent in a analysis of solution and NC formation energies, vacancies are certainly critical to the kinetics of nucleation and growth of the Y-Ti-O enriched nanofeatures. Thus an important future objective will be to carry out well-planned experimental studies of vacancy, O-V and O-O pair concentrations following MA and their recovery during subsequent higher temperature heat treatments.

The long-term goal of our work is to develop more comprehensive thermokinetic models of the nanofeature evolution based on a combination of atomistic methods, including molecular dynamics and kinetic lattice Monte Carlo simulations, closely linked to experiment. This effort will rely heavily on DFT calculations to provide basic parameters, many-body potentials and insight on key mechanisms that must be incorporated in the more comprehensive models.

ACKNOWLEDGMENTS

We thank Chris G. Van de Walle (UCSB) and Brian D. Wirth (UC Berkeley) for stimulating discussions, and gratefully acknowledge the DOE Office of Fusion Energy Sciences for financial support (Grant No. DE-FG03-94ER54275).

[1] G. R. Odette, M. J. Alinger, and B. D. Wirth, Annu. Rev. Mater. Res. **38**, 471 (2008).
[2] T. Yamamoto, G. R. Odette, P. Miao, D. T. Hoelzer, J. Bently, N. Hashimoto, H. Tanigawa, and R. J. Kurtz, J. Nucl. Mater. **367-370**, 399 (2007).
[3] M. J. Alinger, G. R. Odette, and D. T. Hoelzer, Acta Mater. **57**, 392 (2009).
[4] L. S. Vasil'ev and S. F. Lomayeva, J. Mater. Sci. **39**, 5411 (2004).
[5] M. J. Alinger, G. R. Odette, and D. T. Hoelzer, J. Nucl. Mater. **329-333**, 382 (2004).
[6] M. K. Miller, E. A. Kenik, K. F. Russell, L. Heatherly, D. T. Hoelzer, and P. J. Maziasz, Mater. Sci. Eng., A **A353**, 140 (2003).
[7] M. K. Miller, D. T. Hoelzer, E. A. Kenik, and K. F. Russell, J. Nucl. Mater. **329-333**, 338 (2004).
[8] M. K. Miller, D. T. Hoelzer, E. A. Kenik, and K. F. Russell, Intermetallics **13**, 387 (2005).
[9] E. Marquis, Appl. Phys. Lett. **93**, 181904 (2008).
[10] M. Klimiankou, R. Lindau, and A. Moslang, Micron **36**, 1 (2005).
[11] S. Yamashita, S. Ohtsuka, N. Akasaka, S. Ukai, and S. Ohnuki, Philos. Mag. Lett. **84**, 525 (2004).
[12] D. T. Hoelzer, J. Bentley, M. A. Sokolov, M. K. Miller, G. R. Odette, and M. J. Alinger, J. Nucl. Mater. **367-370**, 166 (2007).
[13] C. L. Fu, M. Krčmar, G. S. Painter, and X. Q. Chen, Phys. Rev. Lett. **99**, 225502 (2007).
[14] J. Rawers, R. Krabbe, and D. Cook, Mater. Sci. Forum **318**, 695 (1999).
[15] H. Kishimoto, M. J. Alinger, G. R. Odette, and T. Yamamoto, J. Nucl. Mater. **329-333**, 369 (2004).
[16] B. Q. Zhang, L. Lu, and M. O. Lai, Physica B **325**, 120 (2003).
[17] Y. Ortega, V. de Castro, M. A. Monge, A. Munoz, T. Legue, and R. Pareja, J. Nucl. Mater. **376**, 222 (2008).
[18] The relaxation time, τ, is given by $\tau \approx 1/ZD$ where Z is vacancy sink strength, taken as $10^{15}/\mathrm{m}^2$, and D is the vacancy(-O complex) diffusion coefficient taken as $D \approx 10^{-4} \exp(-1.55/\mathrm{kT})\ \mathrm{m}^2/\mathrm{s}$. Note very high concentrations of vacancies that escape annihilation would precipitate as vacancy clusters or gas bubbles. The recovery of the vacancy clusters is slower than for individual vacancies, but only gas (Ar and, possibly, O_2) bubbles are persistent at temperatures higher than about 1100 °C (Ref. 17).
[19] The ≈26% is the pore volume of close-packed equally sizes spheres. The void fraction of packed powders varies from this limit, and is generally larger.
[20] Transition phases have higher free energies than the equilibrium phases, but they initially win the kinetic alloy decomposition race. One classic example of transition phases (of many) is the lower temperature decomposition sequence that occurs in Al-Cu alloys proceeding as: GP-zone $\rightarrow \theta'' \rightarrow \theta' \rightarrow \theta$, where θ is the equilibrium Al_2Cu phase. Note, that transition phase formation is the rule, rather than the exception, under conditions where the free energy decreases upon their formation is sufficient. For a basic exposition on this topic, see Ref. 35.
[21] G. Kresse and J. Hafner, Phys. Rev. B **47**, 558 (1993); See also G. Kresse and J. Furthmüller, *ibid.* **54**, 11169 (1996); For code details, see G. Kresse and J. Furthmüller, http://cms.mpi.univie.ac.at/vasp/vasp/vasp.html.
[22] G. Kresse and D. Joubert, Phys. Rev. B **59**, 1758 (1999).
[23] J. P. Perdew, K. Burke, and M. Ernzerhof, Phys. Rev. Lett. **77**, 3865 (1996).
[24] R. R. Pawar and V. T. Deshpande, Acta Crystallogr., Sect. A: Cryst. Phys., Diffr., Theor. Gen. Crystallogr. **24**, 316 (1968).
[25] E. S. Fisher and C. J. Renken, Phys. Rev. **135**, A482 (1964).
[26] F. H. Spedding, A. H. Daane, and K. W. Herrmann, Acta Crystallogr. **9**, 559 (1956).
[27] G. Simmons and H. Wang, *Single Crystal Elastic Constants and Calculated Aggregate Properties: A Handbook* (MIT Press, Cambridge, MA, 1971).
[28] R. Kohlhaas, P. Donner, and N. Schmitz-Pranghe, Z. Angew. Phys. **23**, 245 (1967).
[29] I. Jackson *et al.*,J. Geophys. Res. **95**, 21671 (1990).
[30] P. Olsson, C. Domain, and J. Wallenius, Phys. Rev. B **75**, 014110 (2007).
[31] C. C. Fu, F. Willaime, and P. Ordejón, Phys. Rev. Lett. **92**, 175503 (2004).
[32] Web Elements, http://www.webelements.com/.
[33] G. M. Paton and E. N. Maslen, Acta Crystallogr. **19**, 307 (1965).
[34] Y. Jiang, J. R. Smith, and A. G. Evans, Phys. Rev. B **74**, 224110 (2006).
[35] D. A. Porter and K. E. Easterling, *Phase Transformations in Metals and Alloys*, 2nd ed. (CRC, Boca Raton, 1992).